applied sciences

MDPI

Article

Parametric Sensitivity Analysis of Suspension Design Using Response Surface Techniques

Marco Freddi *, Curzio Pagliari * and Leonardo Frizziero

Department of Industrial Engineering, University of Bologna, v.le Risorgimento 2, 40136 Bologna, Italy; leonardo.frizziero@unibo.it

* Correspondence: marco.freddi2@unibo.it (M.F.); curzio.pagliari2@unibo.it (C.P.)

Abstract

The sensitivity analysis for the design of an automotive push-rod suspension is discussed. Conventional iterative design cycles rely heavily on repeated CAD and Finite Element Method (FEM) analyses. Here, the initial design is based on an alternative and uncommon approach. A pre-CAD diagram of the entire vehicle (for FSAE competition) integrated with drivers is fully parameterized. A series of simulations in which the virtual driver inputs are repeated while the geometry of the suspension varies is executed. A database with isolated geometric effects on suspension loads and performance is obtained. By employing multivariate regression techniques, specifically Response Surface Methodology (RSM), the complex (often nonlinear) relationship between design inputs and structural outputs is mapped. The geometric inputs for this optimization include the coordinates that define the lengths and angles of the suspension triangles, the kingpin angle, the hub length, and aerodynamic downforce coefficients. The key performance indicators analyzed include corner exit speed loss, load and force distribution on the tires and main suspension joints, and the roll and pitch angles of the chassis. This methodology allows for the rapid identification of an optimal design configuration, avoiding trial and error and reducing development time and costs. The proposed framework demonstrates how RSM can enable the configuration of an optimal push-rod design with enhanced performance characteristics and improved manufacturing efficiency. Different case studies based on the mentioned input–output are analyzed to validate the approach in a practical manner.

Keywords: efficient suspension design; car digital twin; sensitivity analysis; multivariable design; push-rod

check for updates

Academic Editor: Suchao Xie

Received: 6 October 2025
Revised: 3 November 2025
Accepted: 5 November 2025
Published: 8 November 2025

Citation: Freddi, M.; Pagliari, C.; Frizziero, L. Parametric Sensitivity Analysis of Suspension Design Using Response Surface Techniques. *Appl. Sci.* **2025**, *15*, 11887. https://doi.org/10.3390/app152211887

Correction Statement: This article has been republished with a minor change. The change does not affect the scientific content of the article and further details are available within the backmatter of the website version of this article.

Copyright: © 2025 by the authors. Licensee MDPI, Basel, Switzerland. This article is an open access article distributed under the terms and conditions of the Creative Commons Attribution (CC BY) license (https://creativecommons.org/licenses/by/4.0/).

1. Introduction

Automotive engineering research has historically focused on vehicle design, especially its dynamic behavior. Conventional methods primarily focus on macroscopic factors such as vehicle mass, moments of inertia, wheelbase, track width, center of gravity position, and shock absorber properties (stiffness, damping, and mounting points) [1,2]. Unquestionably, these characteristics are essential for comprehending and forecasting basic dynamic phenomena such as pitch, roll, rollover tendency, and sliding [3,4]. Considerable progress has been achieved in optimizing these traditional characteristics, frequently using complex techniques that range from the incorporation of mechatronic components for comfort enhancement to optimal design strategies [2]. In recent decades, there has been a growing interest in using artificial intelligence and sophisticated computer methods to improve

safety assessments and vehicle design. Predictive maintenance and thorough system analysis now have more options because of the development of digital twin models [5]. Robust simulations and optimization are made possible by the dynamic, real-time representation of physical systems provided by these models. Simultaneously, the examination of vehicle running safety has evolved significantly in the field of reliability engineering [6,7], frequently incorporating cutting-edge deep learning techniques for trajectory control and dynamic analysis [8]. These studies demonstrate how the tools accessible to designers are becoming more sophisticated and complicated, allowing for more in-depth examinations of how vehicles behave in different scenarios.

Notwithstanding these developments, there is still a significant gap in the methodical examination of less obvious variables related to suspension parts. Although the significance of the overall suspension configuration is widely recognized [1,2], less is generally known about the specific design decisions made at the component level, such as the lengths and angles of the push-rod arms, their orientations, the placement of uniballs, the hub length (and its direct impact on track width), and the exact point at which the push rod is attached to the lower control arm. These decisions have both isolated and combined effects on the overall dynamics of the vehicle. Research is frequently focused on the macroscopic results of suspension design rather than the complex geometric aspects that determine these results [9]. For example, research on resilient optimization or optimal suspension design [1,2] usually ignores the subtle but important effects of these intricate geometric factors by treating the suspension as a black box or oversimplifying its kinematic chains. Comparably, although digital twins are effective [5], there is less information on how they may be used to precisely optimize the geometry of individual suspension components before physical prototyping to identify hidden design factors. The optimization of proven, macroscopic suspension characteristics (such as stiffness, damping, and general architecture) is the main emphasis of other works [10]. The finer geometrical features of suspension parts (such as push-rod arm angles and uniballs placement) and how they specifically affect dynamics are not covered. The driver's role in vehicle dynamics models is also commonly left out or oversimplified in the present studies. It is less typical to integrate an explicit, realistic driver model in the context of suspension design optimization, even if some research uses sophisticated control techniques [11] or vehicle state prediction for autonomous driving [12].

By carefully examining the effects of these "less intuitive" suspending variables, this work directly tackles these noted weaknesses. Our study explores the subtle yet significant impact of geometric elements on vehicle dynamic behavior, in contrast to earlier investigations that mostly concentrate on well-established characteristics. Here, the separate and combined effects of variables such as hub length, push-rod attachment points, uniballs location, and push-rod arm angles are methodically examined. Digital twins [5,13,14], AI for dependability [6–8], and generic vehicle dynamics prediction using AI [15–23] are all covered in several studies. Despite their strength, these studies frequently fail to apply these sophisticated techniques to the issue of pre-CAD optimization. Iterative CAD and physical prototyping are common components of traditional design processes, and they can be expensive and time-consuming. Before actual CAD prototyping, the methodology allows for the prediction of vehicle behavior and the identification of the best suspension setups (Section 3). This results in significant time and cost savings for the design process, enabling designers to arrive at the CAD stage with a highly optimized setup and knowledge.

2. Methodology and Setup

The push-rod suspension is a type of independent suspension system commonly used in high-performance vehicles, particularly in motorsports. Its design is intended to allow for greater control over the vehicle's dynamic behavior. The core of the mechanism involves a push rod that is connected from the lower arm to the rocker using uniballs. The rocker then acts as leverage on a horizontally or vertically mounted spring-damper unit.

This design offers several advantages. By moving the heavy spring-damper unit inboard, away from the wheel, the push-rod system reduces the overall unsprung mass. This improves tire contact with the road [24–26], leading to better grip, handling, and ride comfort. This configuration allows engineers to precisely control the suspension's motion ratio, which defines the relationship between the wheel's vertical movement and the spring's compression. This offers a high degree of tunability for fine-tuning the vehicle's kinematics. As readers may imagine, the design of a push-rod suspension involves many parameters that can be varied to achieve specific performance goals.

Geometric coordinates, lengths, and angles of the suspension triangles are possible design factors. Another one is the kingpin angle, defined as between the steering axis and the vertical axis (points p_1 and p_4 in the figures below). Hub length is the distance from the center of the wheel to the suspension attachment points.

Aerodynamic downforce coefficients are also mentioned here as they are used to simulate the dynamic load on the vehicle from the front and rear wings. The objective function is what the optimization process aims to improve. In this case, the goal is to optimize a generic multivariable function that represents a combination of the following key performance indicators (KPIs). Corner exit speed, load and force distribution on the tires and suspension joints, vehicle stability, and roll and pitch angles are examples of outputs that will be analyzed.

In the context of the RSM, "factors" refers to the process of creating a database of samples based on changes in the configuration of the simulated system and the resulting recorded output changes (unless there is no connection). This study uses several crucial areas to schematize the full push-rod suspension that is currently being built, as depicted in Figure 1.

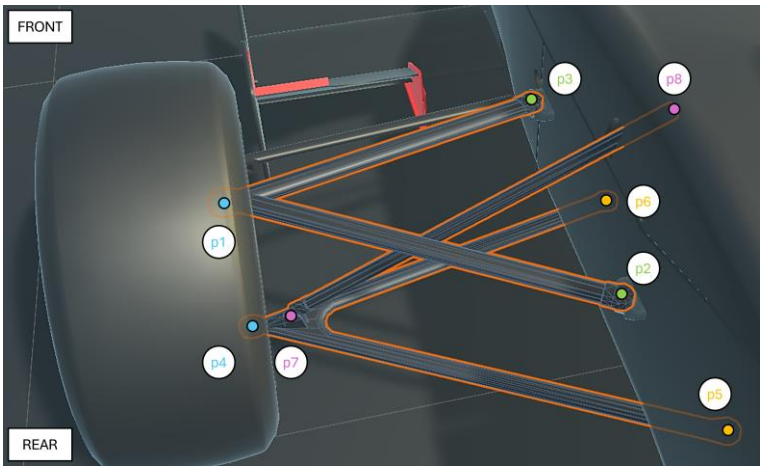

Figure 1. Eight critical points (x,y,z) useful to define the geometry of the front left push-rod suspension.

Every important point and every basic geometry (rods and cylinders) formed between two of these points represents a pre-CAD suspension, known as a scheme. The first seven points (p_1, . . ., p_7) are visible to the readers. The connection between the rocker and the push rod, the rocker and the chassis, and the rocker and the shock absorber generate three

more points (p_8, p_9, and p_{10}). Another point (p_{11}) can be added if the shock absorber's variable orientation inside the monocoque is considered. The real geometry is customizable, and each point has three Cartesian coordinates that can be altered in space. The 11 strategic points are represented by the 33 potential factors for an RSM analysis (and others may be defined).

The foundation of this regression analysis is a mathematical model that attempts to match the point cloud of the dataset by generating a polynomial hypersurface of N terms and order O. Mathematically, this means that at least P trials are needed, where P is equal to (1):

$$P = \binom{N+O}{N} = \binom{N+O}{O} = \frac{(N+O)!}{N!O!} \quad (1)$$

If $N = 33$ and $O = 2$ (2nd-order model), 595 tests are needed in this case. The number may become higher to statistically validate the regression analysis. In fact, 595 is the minimum number of tests (spatial points) required to mathematically define the regression hypersurface. Therefore, it is essential to try to lower N. However, mono-variable analyses cannot lead to the identification of the mixed effects (related to the simultaneous variation of two or more variables, translated into the presence of relevant mixed terms in the polynomial equation of the regression surface).

Readers may opt for a trigonometric parameterization of suspension, which is recommended. This aids in avoiding nonsensical/non-working designs. In Figure 2, a trigonometric method is displayed.

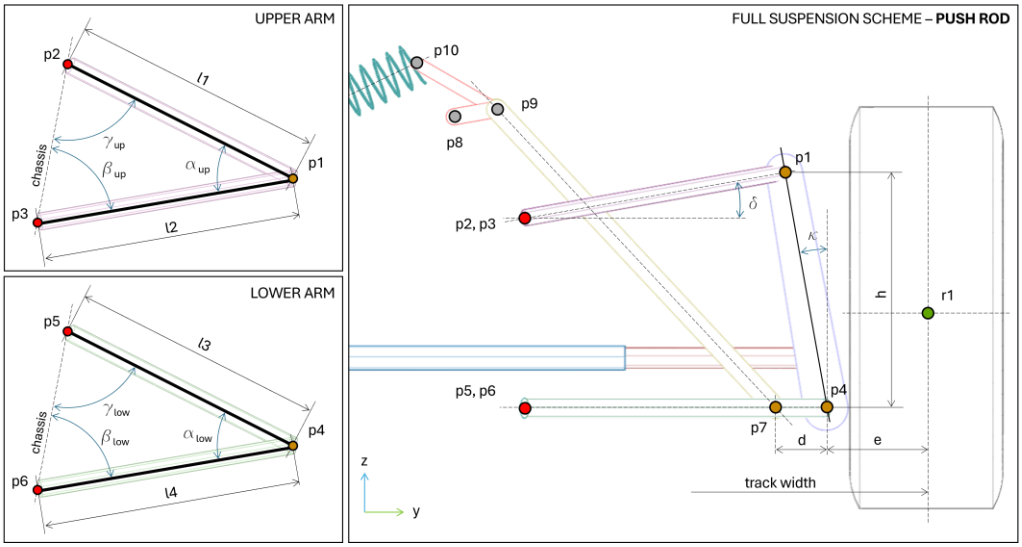

Figure 2. Trigonometric design of push-rod suspension with Lagrangian variables.

The reader is free to customize the parameterization of the model. In the figure, only two of the three angular variables are independent, as, for instance, g is determined by the fluctuation of a and b. Depending on whether the y-coordinates of the four uniballs between the control arms and the chassis are fixed (in this case study, the chassis is already manufactured), l_1 and l_2 dimensions (in Figure 2) may or may not be taken into account. Tire lateral, longitudinal, and radial stiffnesses, wheel and rim diameters, aspect ratios, static and dynamic friction coefficients, wheel rolling resistance, and other variables can all be modeled using UA-tire models. The tire model utilizes a simplified representation of the tire properties (e.g., a basic curve or a simplified Pacejka model) suitable for general dynamic analysis, but it does not account for complex thermal effects or highly nonlinear dynamics at the limit of adhesion.

As stated in the Introduction, a driver model based on Dempster anthropometry is now included in the digital twin of the FSAE vehicle [27,28]. Since drivers account for a significant percentage of total weight, it is essential to consider them in the model with their hypothetical weight distribution. Each body segment is divided into rigid bodies with centers of mass, weights, and moments of inertia like those of a real driver [29,30]. Literature offers different examples related to this topic [28]. To replicate the vibratory impacts and natural movements when driving as much as possible, the driver is attached to the car by suitable bushing joints with variable stiffness and damping, as seen in Figure 3.

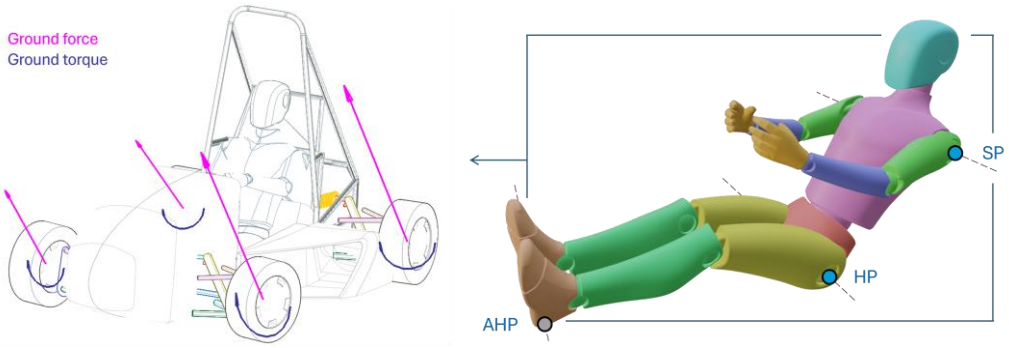

Figure 3. The driver model divided into main segments and integrated into the monocoque to complete the digital twin used in simulations.

In this figure, AHP is the acceleration heel point, HP is the H point, and SP is the shoulder point. These points serve as crucial joints, with three axes of rotation passing through them to represent the main rigid body movements of the virtual mannequin. This model, based on Dempster anthropometry, is integrated into the vehicle's digital twin to more accurately account for the driver's weight and dynamic movements [31].

2.1. Analysis of Variance and Most Influential Variables

The RSM on which the ANOVA is based finds numerous confirmations in the literature [32–40]; they demonstrate its effectiveness in the study of complex systems and in the identification of key design variables. The RSM regression models developed from the test of the generic dataset representative of the system (simulated or real) can be linear or of polynomial order greater than 1. For instance, a 2nd-order polynomial hypersurface follows the following generic Equation (2):

$$y = \beta_0 + \sum_{i=1}^{k} \beta_i x_i + \sum_{i=1}^{k} \beta_{ii} x_i^2 + \sum_{i<j} \beta_{ij} x_i x_j + \epsilon \quad (2)$$

The weights β_i must be identified based on the fit with the point cloud in the database. If the effects of the N factors are only linear, the model can be reduced to a hyperplane. The Pearson correlation coefficient in a mono-variable analysis is expressed by (3):

$$R^2 = \frac{\sum_{i=1}^{n}(x_i - \overline{x})(y_i - \overline{y})}{\sqrt{\sum_{i=1}^{n}(x_i - \overline{x})^2} \cdot \sqrt{\sum_{i=1}^{n}(y_i - \overline{y})^2}} = \frac{\mathrm{Cov}(X,Y)}{\sigma_X \sigma_Y} \quad (3)$$

Here, x_i and y_i are input and output vectors, $\overline{x}$ and $\overline{y}$ the average values, and n the number of tests. Since the study is rigorous and impacted by a low computation error rate, high coefficients are expected (even in the 95–98% range).

Several design models can be used to build the final database for the ANOVA model. The full factorial design entails modeling every possible combination, M^N, if N factors (inputs), each of which is made to vary M times (levels), are considered. A reduction

in testing is possible with other designs, such as the Box–Behnken design, the Central Composite Design (CCD), the Doehlert design, and Latin Hypercube Sampling (LHS), although the dependability is typically lower. Although random factor level generation can also be effective, a balanced investigation of the domain cannot be ensured with a few trials. Because of this, it would be beneficial to obtain real-time data from physical simulations or, based on the concept in the Introduction, virtual simulations. Tests conducted using single mono-variable simulations cannot compare to the volume of data generated by live-time telemetry. The vehicle's virtual model is then tested by reconstructing circuits with bends that have different speeds and turning radii. The car is driven multiple times with limited braking and at top speed (about 100 km/h).

2.2. Optimization Methodology

When the RSM design is selected (CCD, full factorial, Doehlert, ...), the process is carried out as follows. A high number (500 here; readers may opt for a higher value of tests) of simulations on the vehicle's digital twin is performed to generate the dataset. In each simulation, design variables (inputs) are strategically varied, recording the corresponding performance outputs. The database is then subjected to an ANOVA; Pareto charts and Normal plots are generated together with the final regression equation and table of p-values. These visual tools highlight the most influential design variables and those with minimal impact, focusing the optimization process on the key variables.

A second-order (or higher) polynomial regression model is generated at the end. The choice of a second-order model is crucial for capturing the nonlinearities and interactions between variables that a linear model would fail to detect. Defining the regression model means identifying the β_{i} coefficients of the following system (4):

$$\begin{aligned} y_1 &= \beta_0 + \beta_1 x_{11} + \beta_2 x_{12} + \ldots + \beta_k x_{1k} + \varepsilon_1 \\ y_2 &= \beta_0 + \beta_1 x_{21} + \beta_2 x_{22} + \ldots + \beta_k x_{2k} + \varepsilon_2 \\ &\vdots \\ y_n &= \beta_0 + \beta_1 x_{n1} + \beta_2 x_{n2} + \ldots + \beta_k x_{nk} + \varepsilon_n \end{aligned} \tag{4}$$

Output y_{i} is calculated based on input x_{nk} and weights. The system can be rewritten in matrix form (5):

$$y = \begin{bmatrix} y_1 \\ y_2 \\ \vdots \\ y_n \end{bmatrix}$$
$$X = \begin{bmatrix} 1 & x_{11} & x_{12} & \ldots & x_{1k} \\ 1 & x_{21} & x_{22} & \ldots & x_{2k} \\ \vdots & \vdots & \vdots & \vdots & \vdots \\ 1 & x_{n1} & x_{n2} & \ldots & x_{nk} \end{bmatrix} \tag{5}$$

Finally, it is possible to calculate the β_{i} factors using the following Formula (6):

$$\left(X^T X\right)^{-1} X^T y = \begin{bmatrix} \beta_0 \\ \beta_1 \\ \beta_n \end{bmatrix} \tag{6}$$

This model easily avoids overfitting, as the curvature of the regression space remains constant. The polynomial enables the identification of optimal or sub-optimal configurations. These configurations are mathematically pinpointed by searching for points

with a zero gradient, where the regression model predicts the best performance for the desired outputs (7).

$$\nabla f(x_1, x_2, \ldots, x_n) = \vec{0} \quad (7)$$

∇f is the symbol of the gradient, a vector operator that contains all partial derivatives of a function. Then, $f(x_1, x_2, \ldots, x_n)$ is the objective function, and $x_1, x_2, \ldots, x_n$ are the input variables, i.e., the suspension design parameters (e.g., kingpin angle, hub length, and so on). More details about DOE, RSM, and ANOVA are in [41].

In summary, this optimization method is not limited to a manual iterative process. It leverages the power of simulations to build predictive models guiding the identification of the most efficient suspension setup, relying on a suite of established software and modeling approaches. The core of the analysis is built on commercial proprietary software for dynamic simulation (Nx Motion v. 39.0, used here, or others such as Recurdyn, Adams, Matlab), which is used to create and test the high-fidelity 3D digital twin of the vehicle and suspension. The vast database generated from these simulations is then processed using RSM/ANOVA analysis software (such as Minitab or Design Expert) to construct the predictive polynomial regression model, utilizing a standard commercial license. The digital twin integrates a Dempster anthropometry-based driver model, developed based on the established literature, to accurately account for the driver's dynamic mass distribution. Finally, the model incorporates a simplified version of standard UA-tire models to simulate tire–road contact forces, ensuring applicability to general dynamic analysis without adding the complexity of nonlinear thermal effects.

3. Results

In the first analysis, the vehicle performs the same types of curves (J-shape and slalom) with variable radii, curvatures, and speeds. The driver's behavior remains unchanged. This allows for the detection of dynamic fluctuations that are sensitive to changes in the geometric inputs throughout the experiments. A visualization of the single-seater's inputs is shown in the graph in Figure 4.

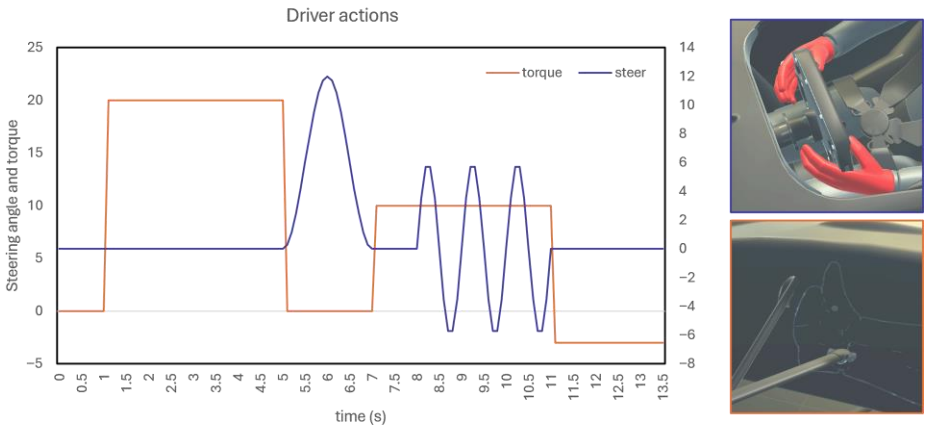

Figure 4. First example of the driver's input telemetry kept constant during simulations.

The vehicle is subjected to a range of testing and operating modes to highlight all significant loads and investigate all the anticipated behaviors. Figure 4 illustrates the driver's J-trajectory. Other tests involve twisting, slaloming, steering, and acceleration. The main outputs are acceleration and braking durations, the maximum roll angle measured, the end speed, the position of the chassis (x; y) on the ground plane (trajectory), the direction of the speed vector at the end of each curve (yaw angle, to obtain information on oversteer and understeer), and the forces in the main suspension joints ($F_1, \ldots, F_{11}$). All simulations

assume an ideal, flat, and dry road surface with consistent friction properties. The influence of varied road roughness, imperfections, or wet/low-grip conditions is not considered.

3.1. Analysis of the Variation in Individual Variables on Specific Outputs

It is not possible to provide every single result here. Some example results are shown. The reader is free to customize their analysis. For instance, Figure 5 shows that the variation in the kingpin angle alters the force peaks occurring on the relative uniballs, despite the vehicle inputs and the way they curve always being the same. In fatigue sizing, this effect must be weighed together with those related to performance.

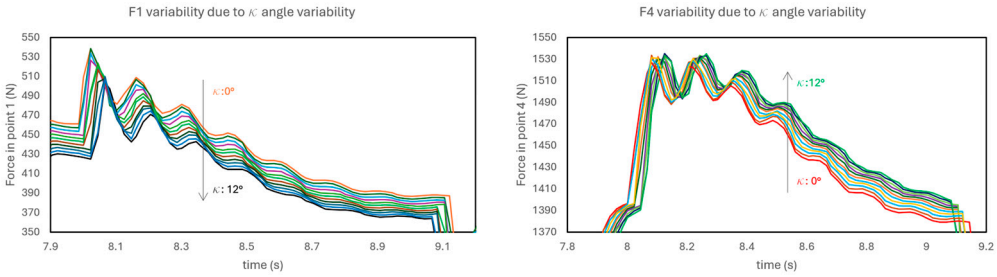

Figure 5. Force on spherical linkages 1 and 4 (arms–knuckle) varying with kingpin angle.

The transverse load transfers (between the wheels inside and outside the curve) clearly change when the vehicle's width (t) is changed. Road holding, grip, and tire-to-ground contact are all impacted by these factors. However, excessive load transfers run the danger of decreasing the inside wheels' grip on the bend, making it harder to steer and maintain the curve.

At the same time, by varying the angle d (this is the measurable angle of the upper arm when the vehicle is stationary; see Figure 2), the compression force F7 of the push-rod element changes, discharged directly on the shock absorber. This undoubtedly alters the stability of the vehicle. In modern F1 cars, the upper arms are often angled upwards ("anedrons") at the point of attachment to the chassis. This inclination is mainly dictated by aerodynamic reasons, allowing for cleaner airflow under the bottom of the car, which is crucial for generating downforce. However, they also have a net effect on the change in camber of the tire during curved trajectories. These last two aspects are graphed in Figure 6.

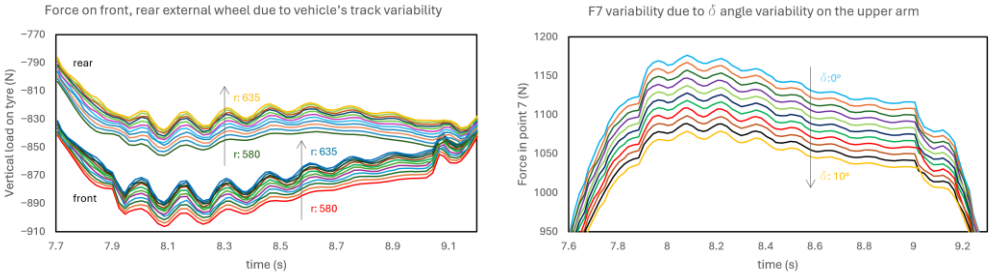

Figure 6. Alteration of load transfers and push-rod force due to geometry changes.

An example of ideal control, according to the authors, involves changing the maximum translation of the steering rack during the curve. For example, in Figure 7, it is notable how entering a curve at a constant initial speed (avoiding accelerating/braking during execution) changes the exit speed as the turning radius changes. Here, the vehicle begins to steer at 7 s, for 3 s, reaching the maximum steering rack translation at 8.5 s. The kinetic energy lost by the vehicle is therefore measured in a "pure" way, depending only on geometry and steering, without the intervention of accelerating or braking effects.

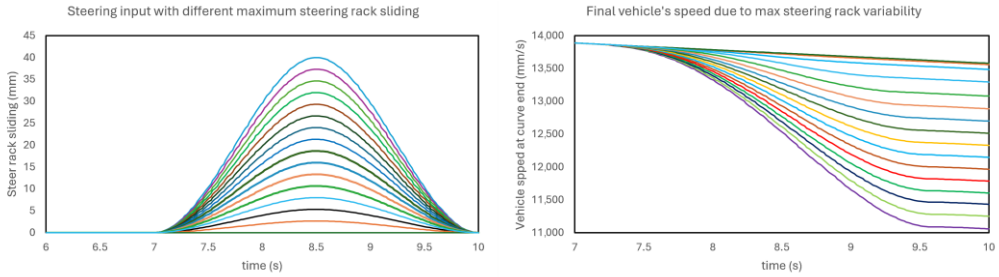

Figure 7. Kinetic energy is lost by the vehicle when cornering due to the different turning radii.

From the two graphs, when the vehicle does not steer, the losses of kinetic energy and speed are linear and depend on friction with the ground (in the absence of aerodynamic loads). This situation is represented by the horizontal curve (zero) in the steering input graph and the highest curve in the final velocity fraction analyzed. Increasing the turning radius then causes more slowdown as indicated. When cornering, other interesting effects are observed. For example, S-curves (slalom) allow for the identification of further links between design variables and outputs. For example, Figure 8 shows the effect on the roll angle and camber angle of the front wheel linked to the maximum translation of the steering rack (tsr in the figures; measured in mm). It is noticeable that even in this case, a physical limit is reached because the curves tighten within a sinusoidal boundary as the maximum steering increases. Beyond those values, the vehicle and the tires do not go, and a loss of grip will probably happen.

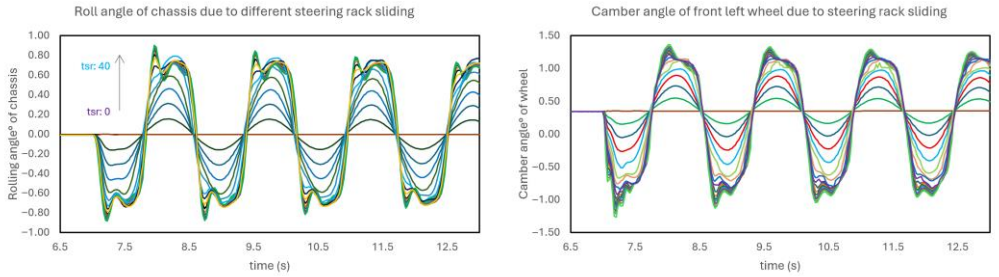

Figure 8. Rolling angle on chassis and camber angle variation in FL wheel due to different maximum steering radii.

Similarly, Figure 9 shows vertical and lateral forces recorded on the tires during the slalom. In this case, the grip limits have been reached too, and the suspension will not suffer higher loads due to curvature. The force limits that the suspension components will undergo are identified at this point. Beyond these limits, the vehicle will lose grip.

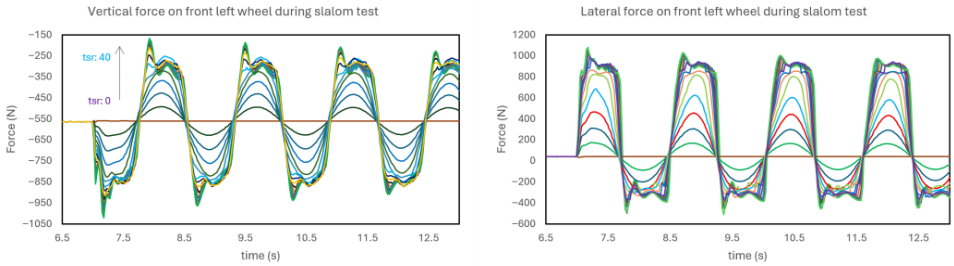

Figure 9. Vertical and lateral load on front left wheel during slalom (adherence limit).

In a rigid body model, it is challenging to integrate information related to fluid dynamics, as the two domains are often treated separately. However, if drag and downforce coefficients (c_d and c_l) of an aerodynamic component of the vehicle (such as front wing, rear wing, spoiler, etc.) are known from CFD analyses, it is possible to define forces acting at the

centroids of these elements to account for their effects, calculated based on the change in vehicle speed, as in (8).

$$\begin{cases} F_d = \frac{1}{2}\,\rho\, c_d\, A\, v^2 \\ F_l = \frac{1}{2}\,\rho\, c_l\, A\, v^2 \end{cases} \tag{8}$$

Here F_i is the drag or lift force on the vehicle, ρ is the density of the air fluid, c_i is the drag (first equation) or downforce (second equation) coefficient, A is the area of impact of the vehicle, and v the relative velocity between the vehicle and the flow, calculated in each frame of the simulation. For example, in some dynamic characterization tests, a front wing was added to the vehicle, and the downforce coefficient was varied. Complex airflow interactions or transient aerodynamic changes due to vehicle pitch and roll are considered simplifications of the real-world scenario. The increased load on the front axle enhances the vertical force and the grip of the front tires. As a result, the lateral force generated by the tires also increases accordingly. Figure 10 shows the trends related to this effect.

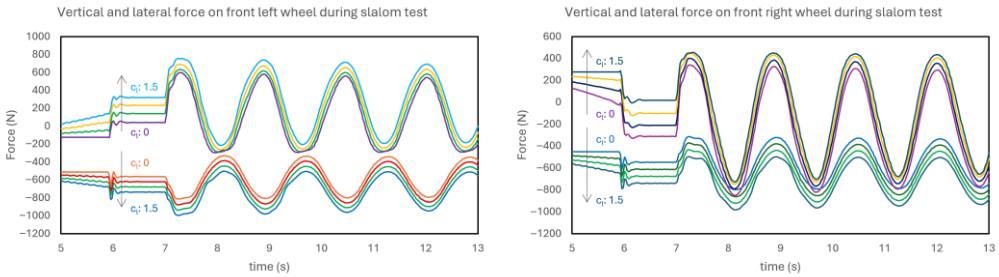

Figure 10. Vertical and lateral loads on front left and right wheels vary with c_l (0–1.5).

It is clearly observed that as c_l increases from 0 (absence of aerodynamic element) to 1.5, both the loads involved and the vehicle's grip properties improve. Similar tests allow for the analysis of additional results, such as the effect of c_l on the vehicle's lateral slip velocity or on the self-aligning moment of the wheels. In the first of the two plots (Figure 11), the steering wheels anticipate the peaks in slip velocity by a few tenths of a second. If the front (steering) wheels experience greater slip, the slipping effect on the rear wheels is consequently slightly reduced. In the self-aligning moment plot in Figure 11, it is also evident that the grip limits of the tires are reached, resulting in a drop in aligning torque during moments of maximum curvature. In these simulation instances, the wheel loses lateral adherence.

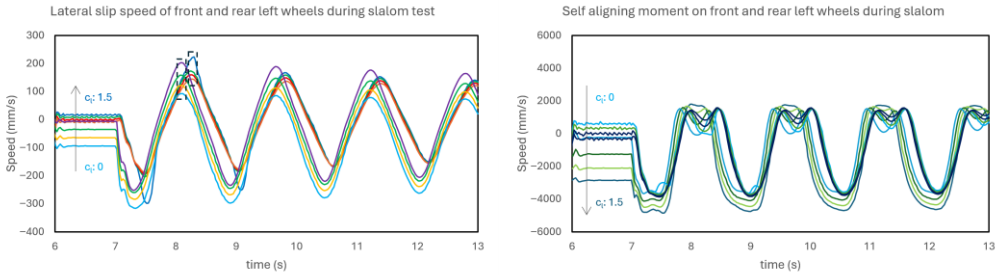

Figure 11. Lateral slip speed and self-aligning moment varying with the c_l coefficient (0–1.5).

3.2. Multivariational Analysis of Ten Variables on the End-of-Curve Velocity

To sum up, comprehensive vehicle mapping is useful to identify several key parameters to define suspension behavior. As the most important variables are mapped, the suspension's behavior is predictable. Some of the design variables' (not related to the driver or engine) most influential impacts on the outputs are identified in the following list: κ, δ_{up}, β_{up}, γ_{up}, h, r_x, δ_{low}, β_{low}, γ_{low}, and d. They are already described in Figure 2 and characterize the geometry and mounting of the two suspension arms and the hub

carrier. An initial configuration of the vehicle is not defined because simulations can be immediately used to generate the database. On the other hand, a range of variations can be defined: [0°; 12°] per κ, [0°; 10°] per δ_{up} and δ_{low}, [60°; 70°] per β_{up} and β_{low}, [60°; 70°] per γ_{up} and γ_{low}, [185 mm; 235 mm] per h, [590 mm; 680 mm] per r_x, and [10 mm; 100 mm] per d.

The system needs to be sampled with numerous tests to find any second, third, or more nonlinearities. For this reason, 500 J-curve tests are carried out by randomly varying the values of the ten variables (respecting the range for each). Tests are set up as previously described. The simulations are set in an automated way with Nx Motion, but readers are free to use different simulation software. Pareto diagrams related to corner exit speed are displayed in Figure 12 to help identify the design elements that have the most effect on the vehicle's behavior around curves (using the Matlab DOE module or commercial software like Minitab or Design Expert). It is clear to the reader that comparable evaluations can be conducted for each of the design's outputs (all F_i forces, roll and pitch angles, and pneumatic load transfers).

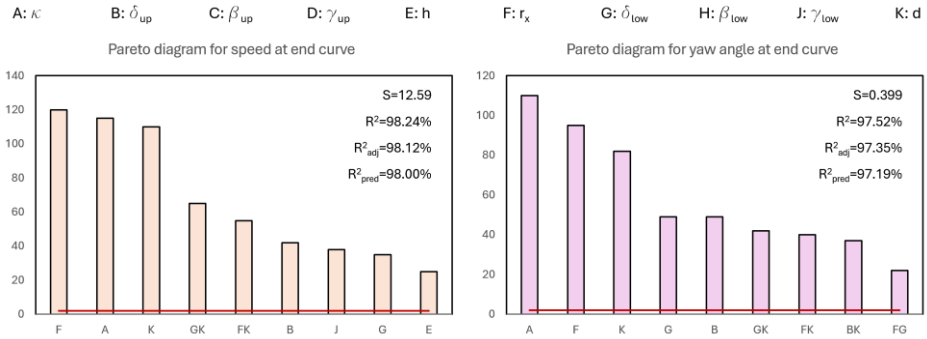

Figure 12. Pareto charts related to the main effects on final speed and yaw at the end curve of the vehicle.

The high correlation coefficients (Figure 12) derived from the model suggest that it is reliable. Limiting the multivariable regression to the second order is certain to exclude possible overfitting situations.

The prime gradient of the resultant n-dimensional hypersurface can be studied since it is composed of a polynomial equation. Local maximums or minimums are anticipated at zero locations, and these serve as the design's references.

It is possible to set a speed-maximizing target on the angle of exit from a particular curve (or set of curves) if the primary goal is to ensure that there is no under- or oversteering. For instance, a first optimal design solution can be achieved by optimizing steering, as seen in Figure 13. This design input configuration optimizes steering, maximizing corner exit speed and ensuring good balance between front and rear slip angles, ensuring no oversteering/understeering.

Optimal configuration (example)

κ	3°	r_x	590 mm
δ_{up}	10°	δ_{low}	3.6°
β_{up}	60°	β_{low}	70°
γ_{up}	70°	γ_{low}	60°
h	185 mm	d	100 mm

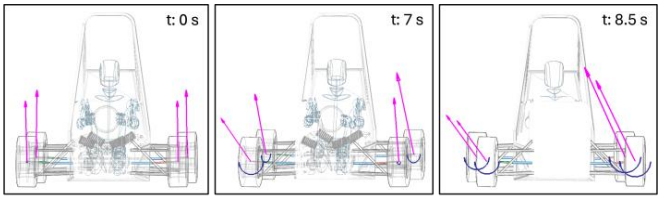

Figure 13. An optimal solution for a specific aim (optimize steering speed during the slalom test) and three frames extracted by the final animation (post-calculation).

The numerical values of these design parameters satisfy the zero-gradient condition of the RSM model according to the equations already mentioned in paragraph 2. The reader

is free to define a specific RSM template to optimize a different output. As can be deduced from the table, a low kingpin angle (κ=3°) is advisable. The upper angle β_{up} is optimal if set to the minimum, with the lower angle set to the maximum. This can lead the designer to extend the range of analysis (however, this is limited by spatial constraints between chassis and bodywork).

4. Discussion

The findings presented in the previous section demonstrate how the geometry of suspension components directly influences vehicle dynamics under various operating conditions. Unlike traditional black-box suspension models, this study isolates and quantifies the effects of specific geometric variables, such as track width, push-rod angles, and uniballs placement, on critical outputs like roll angle, lateral load transfer, and wheel force distribution. This granularity enables a deeper understanding of how small geometric changes propagate through the system and affect performance. The high correlation coefficients obtained in the RSM and ANOVA analyses validate the predictive power of the regression surfaces, confirming that nonlinear dependencies exist between input variables and performance metrics. For instance, the observed nonlinearity between the steering rack stroke and both roll angle and camber angle reveals an upper boundary beyond which increasing steering input results in no further performance gain and may even induce tire grip loss. This effect aligns with theoretical tire models and real-world observations, where excessive steering leads to diminishing returns in lateral force generation due to slip saturation. Additionally, the integration of aerodynamic forces modeled through downforce coefficients derived from CFD data further illustrates how suspension optimization cannot be decoupled from vehicle aerodynamics. The results highlight how increased front axle load enhances grip but also shifts dynamic balance, affecting slip velocities and self-aligning moments. This indicates that geometry optimization should ideally be performed in conjunction with aerodynamic and chassis-level considerations. Another important aspect emerging from the simulations is the effectiveness of a comprehensive digital twin model that includes a driver representation. By accounting for driver-induced load variations and dynamic interactions, the results more accurately reflect real driving scenarios, where the interplay between human and machine is non-negligible.

The multivariate regression framework also provides a useful tool for early-stage design. By analyzing Pareto charts and hypersurface gradients, designers can identify dominant variables and their optimal ranges without the need for exhaustive CAD iterations. This methodology is particularly valuable in performance-driven contexts, such as motorsports, where design cycles are constrained by time, and minor performance gains can yield significant competitive advantages. Future improvements could include the integration of time-dependent variables, such as damper rates and real-time aero adjustments, or the coupling of the digital twin with machine learning agents capable of simulating diverse driving styles and adapting setup recommendations accordingly. It is important to note that the effectiveness of the method is also based on the reliability of simulation software (commercial or non-commercial), whose accuracy is generally validated in the literature [42–47] but certainly requires physical validation in every project. The very existence of such tools and their widespread use in the automotive and racing industries confirm the validity of predictions based on virtual models.

The proposed model and methodology possess high applicability in real-world product development, specifically targeting the early-stage conceptual design (pre-CAD) phase. Its primary value lies in its capability to efficiently optimize critical geometric parameters (e.g., track width and kingpin angle) before committing resources to detailed CAD modeling and physical prototyping. This approach yields a significant reduction in devel-

opment time and cost. While the model effectively identifies the relative optimum within the defined design space, the results serve as high-value input for subsequent advanced design engineering (CAD/FEM). Due to necessary simplifications (e.g., simplified tire and aerodynamic models), the final design derived from this study requires subsequent experimental validation on a physical prototype to confirm absolute performance metrics under real-world driving conditions. Future developments may involve the experimental validation of the optimized design on a physical prototype, integration of advanced nonlinear tire models (e.g., full Pacejka) to enhance prediction fidelity at adhesion limits, and aero-suspension interaction optimization by including more complex aerodynamic design variables. Furthermore, the enhancement of driver model fidelity to incorporate driver perception and control response may be considered, with the development of real-time suspension adaptation strategies using RSM-derived sensitivity maps and telemetry data.

5. Conclusions

This study shows how a vehicle's dynamic behavior can be significantly impacted by the suspension system's many geometric factors. Prior to any CAD modeling, we determined the most important design parameters using a systematic approach that combined single-variable and multivariable simulations on a full-vehicle digital twin (with an integrated driver model).

The vehicle's track width was found to be one of the most important factors affecting load transfer and roll behavior during cornering, supporting theoretical predictions among the variables examined. Additionally, there was a noticeable impact from the upper control arm's kingpin angle and inclination, especially on camber behavior and force distribution at suspension joints. Furthermore, nonlinear interactions and linked effects that would otherwise be impossible to detect through isolated testing were discovered through the combination of ANOVA and RSM.

Further improving simulation realism and guaranteeing that outcomes take into consideration the linked nature of driver–vehicle dynamics was achieved through the incorporation of a Dempster-based driver model. By using this method, designers can achieve a high level of setup optimization prior to a physical prototype, which saves money and time during the early stages of development. This approach might be expanded on in future research to incorporate track-specific aerodynamic interactions, telemetry-data-driven real-time adaptation tactics, or experimental validation on prototypes with telemetry. Both racing and production vehicle development benefit greatly from the overall technique, especially when rapid iteration and system-level optimization are needed.

Author Contributions: Conceptualization, M.F. and C.P.; methodology, M.F.; software, M.F.; validation, C.P. and L.F.; formal analysis, L.F.; investigation, M.F.; resources, C.P.; data curation, M.F.; writing—original draft preparation, M.F.; writing—review and editing, C.P.; visualization, L.F.; supervision, L.F.; project administration, L.F.; funding acquisition, L.F. All authors have read and agreed to the published version of the manuscript.

Funding: This research received no external funding.

Institutional Review Board Statement: Not applicable.

Informed Consent Statement: Not applicable.

Data Availability Statement: The raw data supporting the conclusions of this article will be made available by the authors upon request.

Acknowledgments: The authors have reviewed and edited the output and take full responsibility for the content of this publication.

Conflicts of Interest: The authors declare no conflicts of interest.

Abbreviations

The following abbreviations are used in this manuscript:

RSM	Response Surface Methodology
CAD	Cad-Aided Design
ANOVA	Analysis of Variance
CCD	Central Composite Design
LHS	Latin Hypercube Sampling

References

1. Fang, J.; Gao, Y.; Sun, G.; Xu, C.; Li, Q. Multiobjective Robust Design Optimization of Fatigue Life for a Truck Cab. *Reliab. Eng. Syst. Saf.* **2015**, *135*, 1–8. [CrossRef]
2. Kolta, M.M.H.; Mansour, N.A.; Lashin, M.; Soliman, A.M.A. Optimal Layout of Suspension System Employing Mechatronic Inerter for Comfort Enhancement Based on Structure-Immittance Approach. *SAE Int. J. Veh. Dyn. Stab. NVH* **2024**, *8*, 409–425. [CrossRef]
3. Dwivedi, V.D.; Wahi, P. Influence of Gravity on the Vibration Characteristics of a Geometrically Nonlinear McPherson-Suspension Model. *Multibody Syst. Dyn.* **2024**, *61*, 571–596. [CrossRef]
4. Joubert, N.; Boisvert, M.; Blanchette, C.; St-Amant, Y.; Desrochers, A.; Rancourt, D. Frame Loads Accuracy Assessment of Semianalytical Multibody Dynamic Simulation Methods of a Recreational Vehicle. *Multibody Syst. Dyn.* **2020**, *50*, 189–209. [CrossRef]
5. Wan, C.; Li, W.; Yang, B.; Ling, S.; Fu, G.; Hong, Y. Digital Twin Model and Platform Based on a Dual System for Control Rod Drive Mechanism Safety. *Reliab. Eng. Syst. Saf.* **2025**, *261*, 111075. [CrossRef]
6. Lou, P.; Shi, T.; Yang, T.Y. Reliability Analysis for Running Safety of Vehicle on Slab Track via an Improved Second-Order Fourth-Moment Approach. *Reliab. Eng. Syst. Saf.* **2025**, *253*, 110555. [CrossRef]
7. Tang, X.; Cai, X.; Wang, Y.; Wang, P.; Yang, F. Advanced VTSDREF for Vehicle-Turnout System Dynamic Reliability Analysis: Integration of Hybrid Deep Learning and Adaptive Probability Density Evolution Method. *Reliab. Eng. Syst. Saf.* **2025**, *256*, 110762. [CrossRef]
8. Ji, Y.; Huang, Y.; Yang, M.; Leng, H.; Ren, L.; Liu, H.; Chen, Y. Physics-Informed Deep Learning for Virtual Rail Train Trajectory Following Control. *Reliab. Eng. Syst. Saf.* **2025**, *261*, 111092. [CrossRef]
9. Archut, J.L.; Corves, B. Real-Time Multibody Simulation of Vehicle Wheel Suspensions of Different Topologies with Elastokinematic Properties. *Multibody Syst. Dyn.* **2024**, *63*, 255–271. [CrossRef]
10. Gobbi, M.; Mastinu, G.; Doniselli, C.; Guglielmetto, L.; Pisino, E. Optimal & Robust Design of a Road Vehicle Suspension System. *Veh. Syst. Dyn.* **1999**, *33*, 3–22. [CrossRef]
11. Kabzan, J.; Hewing, L.; Liniger, A.; Zeilinger, M.N. Learning-Based Model Predictive Control for Autonomous Racing. *IEEE Robot. Autom. Lett.* **2019**, *4*, 3363–3370. [CrossRef]
12. Nie, X.; Min, C.; Pan, Y.; Li, K.; Li, Z. Deep-Neural-Network-Based Modelling of Longitudinal-Lateral Dynamics to Predict the Vehicle States for Autonomous Driving. *Sensors* **2022**, *22*, 2013. [CrossRef]
13. Botín-Sanabria, D.M.; Mihaita, S.; Peimbert-García, R.E.; Ramírez-Moreno, M.A.; Ramírez-Mendoza, R.A.; Lozoya-Santos, J.d.J. Digital Twin Technology Challenges and Applications: A Comprehensive Review. *Remote Sens.* **2022**, *14*, 1335. [CrossRef]
14. Li, X.; Niu, W.; Tian, H. Application of Digital Twin in Electric Vehicle Powertrain: A Review. *World Electr. Veh. J.* **2024**, *15*, 208. [CrossRef]
15. Chen, J.; Yu, C.; Wang, Y.; Zhou, Z.; Liu, Z. Hybrid Modeling for Vehicle Lateral Dynamics via AGRU with a Dual-Attention Mechanism under Limited Data. *Control. Eng. Pract.* **2024**, *151*, 106015. [CrossRef]
16. Kontos, J.; Bódis, L.; Vathy-Fogarassy, Á. Forecasting Longitudinal Acceleration in Urban Vehicles. *IFIP Adv. Inf. Commun. Technol.* **2024**, *713*, 85–98. [CrossRef]
17. Marotta, R.; Strano, S.; Terzo, M.; Tordela, C. Multi-Output Physically Analyzed Neural Network for the Prediction of Tire–Road Interaction Forces. *SAE Int. J. Veh. Dyn. Stab. NVH* **2024**, *8*, 285–308. [CrossRef]
18. Valente, G.; Perrelli, M.; Adduci, R.; Cosco, F.; Bossio, R.; Mundo, D. Hybrid Physics-Based and Data-Driven Modelling for Vehicle Dynamics Simulation. In Proceedings of the Mechanisms and Machine Science, Turin, Italy, 11–13 September 2024; Springer Science and Business Media B.V.: Cham, Switzerland, 2024; Volume 164, pp. 398–406.
19. Riva, G.; Formentin, S.; Corno, M.; Savaresi, S.M. Experimental Assessment of Neural Networks for Tire-Road Force Estimation. In Proceedings of the 2022 IEEE Conference on Control Technology and Applications (CCTA), Trieste, Italy, 23–25 August 2022; IEEE: New York City, NY, USA, 2022; pp. 658–663.

20. Zhang, B. Intelligent Vehicle Lateral and Longitudinal Decoupled Dynamic Modeling and Control System Simulation Based on GRU-FNN. In Proceedings of the 2024 3rd International Conference on Energy and Power Engineering, Control Engineering (EPECE), Chengdu, China, 23–25 February 2024; IEEE: New York City, NY, USA, 2024; pp. 153–158.
21. Kim, K.-H.; Jeong, C.; Kim, J.; Lee, S.; Kang, C.-M. Neural Network Modeling Approach for Vehicle Lateral Dynamics Using Real Vehicle Data. *J. Inst. Control Robot. Syst.* **2024**, *30*, 696–702. [CrossRef]
22. Kontos, J.; Kranicz, B.; Vathy-Fogarassy, A. Neural Network-Based Prediction for Lateral Acceleration of Vehicles. In Proceedings of the 2022 IEEE 2nd Conference on Information Technology and Data Science, CITDS 2022, Debrecen, Hungary, 16–18 May 2022; IEEE: New York City, NY, USA, 2022; pp. 153–158. [CrossRef]
23. Marinković, D.; Dezső, G.; Milojević, S. APPLICATION OF MACHINE LEARNING DURING MAINTENANCE AND EXPLOITATION OF ELECTRIC VEHICLES. *Adv. Eng. Lett.* **2024**, *3*, 132–140. [CrossRef]
24. Romano, L.; Bruzelius, F.; Hjort, M.; Jacobson, B. Development and Analysis of the Two-Regime Transient Tyre Model for Combined Slip. *Veh. Syst. Dyn.* **2023**, *61*, 1028–1062. [CrossRef]
25. Stocco, D.; Biral, F.; Bertolazzi, E. A Physical Tire Model for Real-Time Simulations. *Math. Comput. Simul.* **2024**, *223*, 654–676. [CrossRef]
26. Liu, Q.; Lu, D.; Ma, Y.; Xia, D. A Novel Numerical Method for Theoretical Tire Model Simulation. *Machines* **2022**, *10*, 801. [CrossRef]
27. Haug, E.; Choi, H.Y.; Robin, S.; Beaugonin, M. Human Models for Crash and Impact Simulation. *Handb. Numer. Anal.* **2004**, *12*, 231–452. [CrossRef]
28. Büchner, S.; Junge, M.; Marini, G.; Fürst, F.; Schick, S.; Peldschus, S. A Priori Prediction of the Probability of Survival in Vehicle Crashes Using Anthropomorphic Test Devices and Human Body Models. *Traffic Inj. Prev.* **2019**, *20*, 544–549. [CrossRef] [PubMed]
29. Pascoletti, G.; Catelani, D.; Conti, P.; Cianetti, F.; Zanetti, E.M. A Multibody Simulation of a Human Fall: Model Creation and Validation. *Procedia Struct. Integr.* **2019**, *24*, 337–348. [CrossRef]
30. Pascoletti, G.; Catelani, D.; Conti, P.; Cianetti, F.; Zanetti, E.M. Multibody Models for the Analysis of a Fall From Height: Accident, Suicide, or Murder? *Front. Bioeng. Biotechnol.* **2019**, *7*, 419. [CrossRef]
31. Macey, S.; Wardle, G.; Gilles, R.; Thomas, F.; Murray, G. *H-Point: The Fundamentals of Car Design & Packaging*; Design Studio Pr, Ed.; Libreria Universitaria: Padua, Italy, 2009.
32. Montalti, A.; Galiè, G.; Pignatelli, E.; Liverani, A. Enhancing Surface Roughness of Material Extrusion Additive Manufacturing Components via an Innovative Ironing Process. *Virtual Phys. Prototyp.* **2024**, *19*, e2401929. [CrossRef]
33. Bacciaglia, A.; Ceruti, A.; Liverani, A. A Design of Experiment Approach to 3D-Printed Mouthpieces Sound Analysis. *Prog. Addit. Manuf.* **2021**, *6*, 571–587. [CrossRef]
34. Bacciaglia, A.; Ceruti, A.; Liverani, A. Investigating Slicing Parameters in FFF for Time and Mass Estimation: A Statistical Approach. *Prog. Addit. Manuf.* **2025**, *10*, 4923–4945. [CrossRef]
35. Liverani, A.; Bacciaglia, A.; Nisini, E.; Ceruti, A. Conformal 3D Material Extrusion Additive Manufacturing for Large Moulds. *Appl. Sci.* **2023**, *13*, 1892. [CrossRef]
36. Dai, W.; Ouyang, Z.; Ji, Y.; Tang, M. Optimization Analysis of Vehicle Dynamic Performance Based on RSM and RBF Approximation Model. *Lect. Notes Electr. Eng.* **2022**, *864*, 363–371. [CrossRef]
37. Zhan, Z.; Fengyao, L.V.; Xin, R.; Zhou, G.; Zhao, S.; He, X.; Wang, J.; Li, J. Automotive Hood Design Based on Machine Learning and Structural Design Optimization. In *SAE Technical Paper*; SAE International: Warrendale, PA, USA, 2023. [CrossRef]
38. Kishore, K.S.; Subbaiah, K.V. Assessment of Optimal Conditions Using RSM Approach: A Case Study on Composites for Automotive Roof Top Applications. *J. Inst. Eng. India Ser. D* **2025**, 1–17. [CrossRef]
39. Veza, I.; Spraggon, M.; Fattah, I.M.R.; Idris, M. Response Surface Methodology (RSM) for Optimizing Engine Performance and Emissions Fueled with Biofuel: Review of RSM for Sustainability Energy Transition. *Results Eng.* **2023**, *18*, 101213. [CrossRef]
40. Chen, H.Y.; Chen, C. A Study of the Response Surface Methodology Model with Regression Analysis in Three Fields of Engineering. *Appl. Syst. Innov.* **2025**, *8*, 99. [CrossRef]
41. Montgomery, D.C. *Design and Analysis of Experiments*; John Wiley & Sons, Inc.: Hoboken, NJ, USA, 2013; ISBN 9781118146927.
42. Yan, X.; Abdel-Aty, M.; Radwan, E.; Wang, X.; Chilakapati, P. Validating a Driving Simulator Using Surrogate Safety Measures. *Accid. Anal. Prev.* **2008**, *40*, 274–288. [CrossRef] [PubMed]
43. Zhang, S.; Zhao, C.; Zhang, Z.; Lv, Y. Driving Simulator Validation Studies: A Systematic Review. *Simul. Model. Pract. Theory* **2025**, *138*, 103020. [CrossRef]
44. Wynne, R.A.; Beanland, V.; Salmon, P.M. Systematic Review of Driving Simulator Validation Studies. *Saf. Sci.* **2019**, *117*, 138–151. [CrossRef]
45. Piancastelli, L.; Frizziero, L.; Donnici, G. Learning by Failures: The 'Astura II' Concept Car Design Process. *J. Eng. Appl. Sci.* **2014**, *9*, 2009–2015.

46. Donnici, G.; Frizziero, L.; Liverani, A.; Buscaroli, G.; Raimondo, L.; Saponaro, E.; Venditti, G. A New Car Concept Developed with Stylistic Design Engineering (SDE). *Inventions* **2020**, *5*, 30. [CrossRef]
47. Frizziero, L.; Rocchi, I.; Donnici, G.; Pezzuti, E. Aircraft Diesel Engine Turbocompound Optimized. *JP J. Heat Mass Transf.* **2015**, *11*, 133–150. [CrossRef]

Disclaimer/Publisher's Note: The statements, opinions and data contained in all publications are solely those of the individual author(s) and contributor(s) and not of MDPI and/or the editor(s). MDPI and/or the editor(s) disclaim responsibility for any injury to people or property resulting from any ideas, methods, instructions or products referred to in the content.